J. Fluid Mech. (1986), *vol.* 167, *pp.* 503–531
Printed in Great Britain

Experimental study of convective structures in rotating fluids

By B. M. BOUBNOV AND G. S. GOLITSYN

Institute of Atmospheric Physics, Academy of Sciences of the USSR, Moscow, 109017, USSR

(Received 6 March 1985 and in revised form 10 February 1986)

We describe a series of laboratory experiments to study convective structures in rotating fluids (distilled water) in ranges of Rayleigh flux number Ra_f from 10^6 to 2×10^{11} and of Taylor number Ta from 10^6 to 10^{12}. An intermediate quasi-stationary ring pattern of convection was found to arise from the interaction of the onset of convection with the fluid spin-up, for which we determined the times of origin and destruction, the distances between the rings, and the diameter of the central ring in terms of Ra_f and Ta. The ring structure evolves into a vortex grid which can be regular or irregular. In terms of Ra_f and Ta the regular grid exists in the linear regime, when the number of vortices N is in accord with the linear theory, when $N \propto h^{-2}Ta^{\frac{1}{3}} \propto \Omega^{\frac{2}{3}}$, or in the nonlinear regime when $N \propto h^{-2}Ta^{\frac{1}{2}}Ra_f^{-\frac{1}{2}} \propto \Omega$, where Ω is the angular velocity and h is the fluid depth. In the irregular regime we always have $N \propto \Omega$. The transition from the regular regime to the irregular one is rather gradual and is determined by the value of the ordinary Rayleigh number, which we found to be greater than the first critical number $Ra \propto Ta^{\frac{2}{3}}$ by a factor about 25–40. In the transition region vortex interactions are observed, which start with rotation of two adjacent vortices around a common axis, then the vortices come closer and rotation accelerates, following which the vortices form a double helix and then coalesce into one stronger vortex.

Some other qualitative experiments show that if the rotating vessel with the convective fluid is inclined to the horizontal, the vortex grid is formed along the rotation axis in accordance with the Proudman–Taylor theorem.

1. Introduction

Convection in rotating fluids is of interest for various applications, but it has not been studied experimentally for a sufficiently wide range of the determining parameters. Jeffreys (1928) was probably the first to note that rotation must increase the flow stability and delay the onset of convection. However, a quarter of a century had passed before the first rigorous results by Chandrasekhar (1953, 1961) and Nakagawa & Frenzen (1955) appeared. These authors found analytically the neutral stability curve for a plane infinite horizontal layer with the free-stress upper and lower boundaries rotating around the vertical axis.

It is known that sufficiently fast rotation of an inviscid fluid forbids motions along the rotation axis (see, e.g. Chandrasekhar 1961) owing to the Proudman–Taylor theorem. However, if the fluid layer is convectively unstable, it needs vertical motions to transfer heat across the layer. There is only one way out of this contradiction: motions are possible in narrow or small regions where the viscosity lifts away the Proudman–Taylor constraint, i.e. in sheets or vortices.

The linear theory of convection in rotating fluids is technically complicated. Analytical results are found only for the free-stress boundaries. Chandrasekhar (1953, 1961) had to use a variational method to find the stability curve and the size of cells numerically. The weakly nonlinear approximation is at present almost intractable (see e.g. Veronis 1968). Therefore, it is difficult to foresee any rapid progress from an analytical approach. The same can be said about direct numerical methods, in view of the rich variety of convective patterns that we have observed and described below.

Therefore, to study this kind of convection, we have performed laboratory experiments. Making full use of our limited facilities and previous experience we have revealed some quantitative characteristics of the processes under study. Qualitative results are presented only to support quantitative ones or where these are unusual. Convection is a simple means of exciting motions in a fluid which reveals some general features of forced motion in rotating fluids and also of vortical motions.

All the experiments were conducted with distilled water, because its parameters and the water itself are readily available over a wide range of temperatures. We have taken the main thermal characteristic of the process to be the total heat flux coming through the fluid layer, f. A method of determining f in the case of the fluid free surface was proposed by Golitsyn (1979) and Golitsyn & Grachev (1980), and it has been tested in a variety of laboratory and field experiments (see Golitsyn & Grachev 1986). Therefore, all our photographic or visual measurements of the flow structure could be classified using the similarity criteria, which are the Rayleigh flux number

$$Ra_f = \frac{\alpha g f h^4}{\rho c_p k^2 \nu}, \tag{1.1}$$

and the Taylor number

$$Ta = \frac{4\Omega^2 h^4}{\nu^2}, \tag{1.2}$$

where α is the thermal expansion coefficient of the fluid used, g the gravitational acceleration, ρ, c_p, k, ν are respectively the density, specific heat capacity at constant pressure, thermodiffusivity and kinematic viscosity, Ω the angular velocity of rotating layer and h its depth. If we know the heat flux f and the temperature of the water T_w we can determine Ra_f with an error of order 5% or less, the main errors arising in calculating f (Grachev 1983; Golitsyn & Grachev 1985). The dependence of all of the parameters on temperature must be taken into account (Vargaftik 1972).

Our work differs from many others when $\Omega = 0$ in that we can determine the Rayleigh flux number, Ra_f, but not the ordinary Rayleigh number, Ra, which is appropriate when the temperature difference between the boundaries ΔT is prescribed. The two numbers are related as

$$Ra_f = Ra\, Nu, \tag{1.3}$$

where the Nusselt number

$$Nu = \frac{fh}{\rho c_p k \Delta T} \tag{1.4}$$

is the ratio of the heat flux f to that which would be in the layer in the absence of motions due to pure molecular conduction. Note that at the stability curve $Nu = 1$ by definition, and therefore, $Ra_{fcr} = Ra_{cr}$ at the curve. Of course, higher up the stability curve we have $Ra_f > Ra$, because there $Nu > 1$.

We know of only three experimental works that contain studies of convection with rotation. Nakagawa & Frenzen (1955) presented some photographs of convective

motions which reveal their vortex structure. They checked the stability curve Ra_{cr} as a function of Ta for water in the range $10^5 < Ra < 10^8$ and $10^6 < Ta < 2 \times 10^{10}$, and gave results of three determinations of the cell sizes at three pairs of values of Ra and Ta. Rossby (1969) concentrated on the influence of rotation on the heat transfer between two rigid plates. He described the spatial structure of convection only at relatively small Taylor numbers, up to 10^4, when the role of rotation is not yet large and he observed rolls which were breaking up into vortices when he increased the rotation further. Dikarev (1983) observed the development of convection in rotating water cooled from above (from the free surface). In his mostly qualitative work, he noted that the convective motions were first organized as concentric rolls which after a time became unstable, and cyclonic vortices were formed in a regular pattern in which the cooled fluid flowed downwards. He found that the time of vortex formation increased with Ω and the number of vortices was also proportional to Ω in accord with the assumption that the distance between the vortices was proportional to the Ekman length

$$l_E = (\nu/\Omega)^{\frac{1}{2}}, \tag{1.5}$$

as was proposed by Golitsyn (1981) for the distance between rolls, or sheets, and by Hopfinger, Browand & Gagne (1982) for vortices forming in a rotating fluid with mechanically produced turbulence. But he did not notice that these results contradicted the linear theory (see (1.10) and §5 below).

An interesting work by Busse & Carrigan (1974), which should also be mentioned here, studied experimentally the convection in an annulus with inner and outer walls heated differentially and applying a very fast rotation so that the centrifugal force was much greater than the gravity force. In the situation when the volume force was almost perpendicular to the direction of Ω they observed convection organized in vertical rolls. This is a good illustration of the Proudman–Taylor theorem.

Before coming to our experiments we present a summary of the main theoretical results (Chandrasekhar 1961; Nakagawa & Frenzen 1955) that we shall need. The critical Rayleigh number for a rotating layer (for Prandtl number $Pr = \nu/k > 0.677$ when there is no oscillating overstability) is

$$Ra_{cr} = 3\pi^4(\tfrac{1}{4} + \cosh\tfrac{1}{3}\phi + \cosh^2\tfrac{1}{3}\phi), \quad \phi = \cosh^{-1}\left(1 + \frac{2Ta}{\pi^4}\right). \tag{1.6a}$$

From this at sufficiently large Taylor numbers (for $Ta > 10^6$ with accuracy better than 1 %) we have

$$Ra_{cr} = 3(\tfrac{1}{2}(\pi^2))^{\frac{2}{3}} Ta^{\frac{2}{3}} \approx 8.7\, Ta^{\frac{2}{3}}. \tag{1.6b}$$

The critical Rayleigh number is related to the critical spatial wave length a_{cr} as

$$Ra_{cr} = 3(a_{cr}^2 + \pi^2)^2, \quad a_{cr}^2 = \pi^2 \cosh\tfrac{1}{3}\phi - \tfrac{1}{3}\pi^2. \tag{1.7}$$

At sufficiently large Ta

$$a_{cr} = (\tfrac{1}{2}\pi^2 Ta)^{\frac{1}{6}} \approx 1.3\, Ta^{\frac{1}{6}}. \tag{1.8}$$

The convective cells have hexagon shapes and the distance between their centres d is related to a_{cr} and the layer depth h by

$$\frac{h}{d} = \frac{\sqrt{3}\, a_{cr}}{4\pi} \approx 0.18\, Ta^{\frac{1}{6}}. \tag{1.9}$$

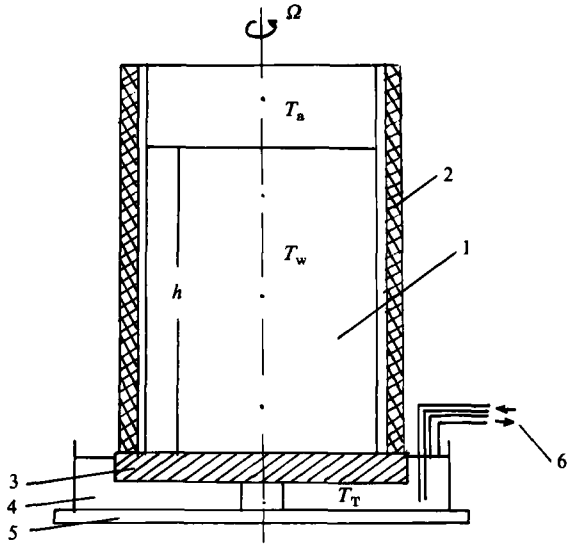

FIGURE 1. A schematic of the experimental installation (see the text for notation).

One can also introduce the vortex density N, which for the hexagonal structure can be defined, using (1.8) and (1.9), as

$$N = \frac{\sqrt{3}}{2} d^{-2} = \frac{3\sqrt{3}}{(4\pi)^2} \left(\frac{\pi^2}{8}\right)^{\frac{1}{3}} Ta^{\frac{1}{3}} h^{-2} \approx 0.028\, Ta^{\frac{1}{3}} h^{-2}. \tag{1.10}$$

The relationships (1.6)–(1.10) were obtained for both free-stress boundaries of the fluid layer and the given temperature difference. But for the problem to be considered here we have the upper boundary free at which not the temperature but the heat flux, is prescribed, i.e. the vertical temperature derivative. To our knowledge no-one has yet considered such a problem. Chandrasekhar (1961) considered cases with two rigid boundaries and one rigid, one free boundary. Though there are no analytical results, inspection of his figures 21 and 22 and tables VII–IX shows that dependences (1.6*b*) and (1.8) apply, with some slight modifications in numerical multiplyers of order a few percent, for a_{cr}. In the range $10^6 < Ta < 10^{10}$ values of Ra_{cr} for both boundaries rigid and both free differ by some 20–15 %, the former being lower than the latter with some decrease in the difference as Ta increases. The case of one rigid, one free boundary is intermediate between the two.

The close agreement of results for Ra_{cr} and a_{cr} for all the three types of boundary conditions allows us to suppose that our particular case with one boundary free and the other rigid with a given heat flux would not differ much from these three cases, as confirmed by the results of §5 with respect to the spatial scale of convection. We did not attempt to determine Ra_{cr} with any meaningful precision but we have assumed in §4 that it would not differ much from the known curves in its dependence on Ta. Thus we shall use the relationships (1.6*b*)–(1.10) as a reference case.

2. Experimental installation and procedure

Laboratory experiments were performed using the installation shown schematically in figure 1. The distilled water was poured into vessel 1, which had two forms. It was either a rectangular vessel of organic glass 1 cm thick with a square bottom

16.4×16.4 cm^2 and 25 cm high, or a cylindrical vessel with internal diameter 17 cm and 21 cm high. Their walls were thermo-insulated by a foamy plastic, 2, which could be removed to give a side view. The bottom, 3, was made of aluminium plate 2 cm thick, and water was circulated through basin 4, from the thermostat, 6. All this apparatus is placed on a turntable, 5, the angular velocity of which could be varied from 0.5 to 5.2 s^{-1} (4.8 to 50 revolutions per minute), though some experiments were carried out at about 1 and 60 rev/min. As a result the Ekman length (1.5) was of order 1 mm or less. At high rotation rates the free-surface slope was noticeable, but this did not introduce any noticeable perturbations in the observed patterns. The cylindrical vessel has a removable lid of double organic glass, through which water from another thermostat could circulate, which was used to perform some qualitative experiments with two rigid boundaries. The shape of the vessel did not in practice influence the convective patterns in the central parts of the vessel, outside the angular regions in the vessel with the square cross-section, so we do not specify it further.

The heat flux in conductive and convective fluids entered the fluid through the aluminium bottom of the vessel from the thermostated water and left the surface by evaporation, thermal radiation and as a sensible heat due to the contact with colder air. The value of the total energy flux in the air equals the total heat flux in the water at stationary conditions, when the temperatures of both media do not change with time. The former was determined using the semiempirical formula (Golitsyn & Grachev 1980, 1986). For the reader's convenience we shall briefly describe the procedure. It is based on the formula

$$f = 0.14 \rho c_p \Delta T_{\mathrm{sa}}^{\frac{4}{3}} \left[\alpha k^2 g \nu^{-1} \left(1 + \frac{m}{Bo}\right)^{\frac{1}{3}} (1 + Bo^{-1}) \right] + \sigma (T_{\mathrm{s}}^4 - T_{\mathrm{a}}^4), \tag{2.1}$$

where the first term on the right is the sum of sensible, f_T, and latent, f_e, heat fluxes in the air above the water surface, and the last term is the thermal radiation flux between the surface and air (or the ceiling). The notations are as follows: ΔT_{sa} is the temperature difference between the water surface and the air well above it (in the room), $m = 0.61 c_p T_{\mathrm{a}}/\mathscr{L}$, $\mathscr{L}$ being the latent heat of water vapour formation at the temperature T_{s} of the water surface. All molecular coefficients are for air at the temperature $\frac{1}{2}(T_{\mathrm{s}} + T_{\mathrm{a}})$ taken from Vargaftik (1972). The Stefan constant $\sigma = 5.67 \times 10^{-8}$ W m^{-2} K^{-4}. The Bowen ratio, the ratio of sensible and latent heat fluxes, is

$$Bo = \frac{f_T}{f_e} = \left(\frac{k}{k_e}\right)^{\frac{1}{2}} \frac{c_p \Delta T_{\mathrm{sa}}}{\mathscr{L} \Delta q} = \left(\frac{k}{k_e}\right)^{\frac{1}{2}} \frac{c_p p (T_{\mathrm{s}} - T_{\mathrm{a}})}{0.622 \mathscr{L} (e_{\mathrm{s}} - e_{\mathrm{a}})} \tag{2.2}$$

where k_e is the coefficient of diffusion of water vapour in the air, Δq the difference of specific absolute humidities at the surface and in the room, p the air pressure, e_{s} and e_{a} are the partial saturation pressures of water vapour, at temperatures T_{s} and T_{a}, q the relative humidity of the room air, and near the water surface we assume $q = 1$. At room temperatures and $T_{\mathrm{w}} \gtrsim T_{\mathrm{a}}$ we always have $Bo \ll 1$, the radiative heat flux is no more than about 10% (Grachev 1983) of the total energy flux (2.1) for the temperatures T_{w} we have used.

We measure the temperature within the water T_{w}, but in (2.1) we have $T_{\mathrm{s}} = T_{\mathrm{w}} - \Delta T_{\mathrm{ws}}$, the last term being the temperature drop across the 'cold film'. It was calculated from Ginsburg & Fedorov (1978) that

$$\Delta T_{\mathrm{sw}} = 2.82 \left(\frac{f}{\rho c_p}\right)^{\frac{3}{4}} \left(\frac{\nu}{\alpha g k^2}\right)^{\frac{1}{4}}, \tag{2.3}$$

where all the quantities are for water. Knowing T_w and T_a, we can calculate ΔT_{wa} and substitute it into (2.1) to get a first estimate of f, which can be used to obtain ΔT_{sw} from (2.3). Then we compute $\Delta T_{sa} = \Delta T_{wa} - \Delta T_{sw}$ and evaluate a new value of the heat flux. It is a process of successive approximations, but, as a rule, one iteration is enough to obtain a precision to within about 1%, or better, in the limit value of the heat flux (the actual value of f would not be as accurate because of the temperature-measurement errors, and there is an error of a few percent in the constant 0.14 in (2.1), Grachev 1983). Golitsyn & Grachev (1986) presented nomogrammes to find the fluxes f_T and f_e, and their sum as functions of ΔT_{wa}, q and T_a which we have used here.

We checked in particular whether there was a decrease in the energy flux from the water surface to the air at large rotation rates Ω and small water depth h. Then convection in the air within the vessel above the water may have a sufficiently high Taylor (and Rayleigh) number and may be influenced by rotation, leading to decreased heat transfer as observed by Rossby (1969) in fluids between rigid plates. To test this we recorded the rates at which the hot water cooled $T_w(t)$ without the lower thermostat 4 at $\Omega = 0$ and $\Omega \neq 0$. Several sets of records of $T_w(t)$ ranging from tens of minutes to several hours at various values of Ω, including $\Omega = 60$ rev/min – our fastest possible rotation, were practically the same for $\Omega = 0$ and $\Omega \neq 0$: differences in $T_w(t)$ were less than 0.2 °C for the same values of t if we started with the same volumes of water and initial temperatures. Because the cooling of water here was determined by the energy flux from the water surface to the air (actually, Grachev 1983 used this technique as one of the tests for (2.1)), we were sure that the rotation did not influence by any appreciable means the value of the heat flux (2.1), which we took in stationary conditions to be the same as the heat flux in water.

We may note here that Nakagawa & Frenzen (1955) observed convection in rotating air in a vessel with the upper lid of sizes several times larger than ours. They observed only three rather large and diffuse vortices and their Taylor number was about two orders of magnitude greater than in our case. Evidently, in our experiments for convection in air in a vessel, which is in free contact with the room air, there is simply 'no room' to organize any flow patterns which could reduce the energy flux from the water surface.

In our experiments the heat flux as determined by (2.1) varied between 5×10^4 and 2×10^6 erg cm^{-2} s^{-1}, or 50–2000 W m^{-2}, and to obtain this we measured only the temperature of the water and dry and wet bulb temperatures of the room. Though the procedure is indeed very simple, it has required in reality very substantial theoretical and experimental efforts to justify it. The reader may be interested to know that the formula (2.1) can be generalized to the cooling of multicomponent solutions (Golitsyn, Grachev & Lapshin 1984). In that paper the generalized formula was checked experimentally for alcohol solutions of various strength by weighing at intervals a vessel containing the solutions on a precise analytical scale, thereby determining the rate of evaporation of both water and alcohol vapours together. The experimental results not only confirmed the general structure of a formula similar to (2.1) for a wide range of the solution temperature and strength, but allowed the determination of the numerical coefficient, which was found to be close to 0.14, within a few per cent. In this connection we note that in the handbook by Martynenko & Sokovoshin (1982) for the free turbulent convection in air for $Ra = 8 \times 10^6$–3×10^{10} over plates with square, rectangular, triangular and round shapes kept at constant temperature with $T > T_a$, the well-known heat transfer law is fulfilled: $Nu = \mathscr{A}\, Ra^{\frac{1}{3}}$ with the constant $\mathscr{A} = 0.15 \pm 0.01$. The formula (2.1) without the radiative term can

be viewed as a generalization of this law, whose physical essence is that the heat flux in convective form does not depend at sufficiently high supercritical Rayleigh numbers on the linear scale of convection.

Other parameters in experiments reported in this paper were varied in the following limits: depth of the water layer h from 2–20 or 24 cm depending on the vessel, temperature of the thermostat water 23–70 °C, room temperature was around 20–23 °C and its relative humidity q varied from 15 to 75 % depending on the season. As a result we were able to study a range of the Rayleigh flux number Ra_f from 10^6 to 2×10^{11} and of the Taylor number from 10^6 to 10^{12}, which are much larger than in the experiments previously published.

The flows were visualized by aluminium powder at the surface or by the dye bromium-thymol blue, whose motion can be easily traced because it dissolves slowly in water. We also sometimes used permanganate particles. The surface of the vessel was photographed and from the pictures obtained linear scales or numbers of vortices were measured.

Specification of the initial conditions is of importance. After filling the vessel (at no rotation) with water of temperature somewhat cooler than the water in the thermostat, we waited for the thermal equilibrium to be established in the volume under study. The water in it is heated from the bottom and cooled from the surface. After some time, the temperature of the water had adjusted to heat supply and losses, and stayed constant throughout the main volume with an accuracy of order of a tenth of a degree, being several degrees colder than in the thermostat. The last fact implies that the heat permanently flows to the water through its vessel's metallic bottom, 3 (see figure 1). At the thermally adjusted state we have never observed thermals rising from the bottom. That means that there was no appreciable, or perhaps it is better to say unstable boundary thermal layer there. But the 'cold film' at the surface apparently caused all the motions in water. The dye brought onto the surface revealed the usual convective patterns in the fluid at rest cooled from the surface (Chernous'ko 1971; Ginsburg *et al.* 1981): cooled within the surface 'film' water sinks along the convergence surfaces often forming irregular polygons. At an intersection of these surfaces a vortex is occasionally formed in which the cooled water sinks more rapidly. It is essentially an irregular regime of convection because our smallest Rayleigh flux numbers were of order 10^6.

After the water temperature ceased to change we switched on the turntable. It reached its chosen constant angular velocity in about a second. Immediately after switching on the rotation the dye formed a spiral on the surface obviously reflecting the spin-up of water. After a time ring structures may appear or vortices in regular or irregular grid patterns. A study of these patterns is the main topic of this paper.

3. Convective rings

Convective rolls as a stationary form of convective motions have also been seen in the absence of rotation for shallow layers in circular vessels with a rigid upper lid (Koschmieder 1967). For large Taylor numbers in deep layers Dikarev (1983) noted that the rings existed for some finite time and afterwards convective vortices were formed. He visualized the motions by a shadow method, directing the light beam vertically through a glass vessel, so that he could see a vertically integrated picture.

We present here the results of a systematic study of the ring convective pattern. Convective rings are formed only if the fluid surface is free and if the rotation axis coincides with the vessel centreline. They do not form if there is an upper lid. They

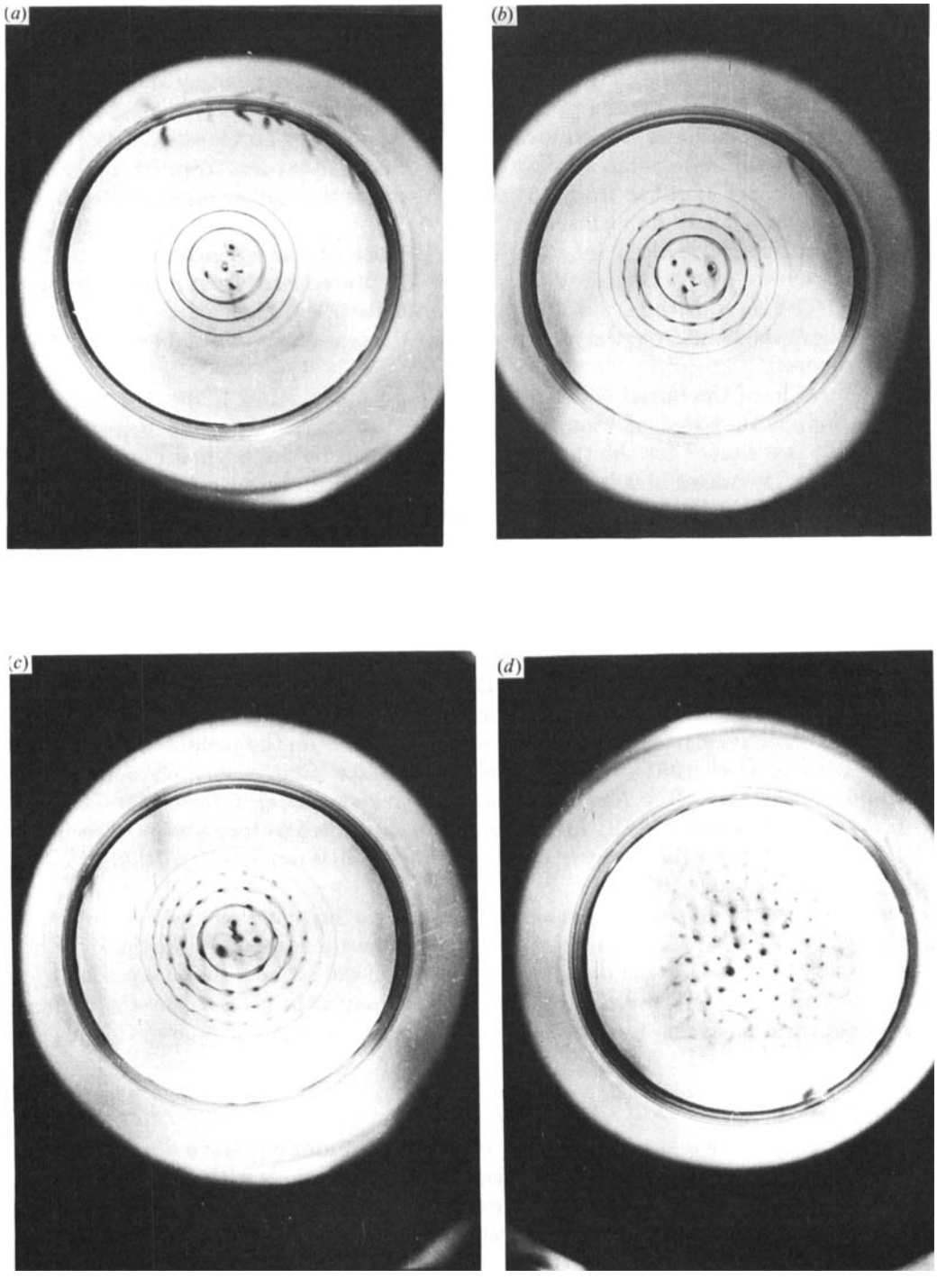

FIGURE 2. Ring convective pattern (*a*) and various stages of its instability (*b*, *c*) leading to the transition to the vortex grid pattern (*d*) at $Ra_f = 3.3 \times 10^7$ and $Ta = 1.9 \times 10^8$.

also do not appear at smaller angular velocities, at $\Omega < 2\ \mathrm{s}^{-1}$ (20 rev/min) in our experiments. But when they do form we observed them in both our vessels: in the square one the rings were inside the circle confined by the square. This means that the boundary layer at the walls does not have any influence on the flow structure. Sometimes at lower heat fluxes we did not see rings near the upper end of our possible rotation velocities, apparently because this was then below the stability curve (1.6*b*).

If the rotation axis is off the centre more complicated forms of cylindrical surfaces can appear. Once we observed an '8-like' structure, but usually there are spirals or parts of spiral-like surfaces. If we stirred the water when a ring pattern was in its initial stage, the convection restored itself in parts of vertical circular or spiral sheets or surfaces. Evidently, the sinking of the colder surface water along the sheets is a preferable mode of convection at initial times and the organization of it in a circular form requires a symmetrical geometry.

The first ring always appears close to the centre in a time τ_{r} after switching on the rotation. A few vortices are seen inside it. Other rings appear one by one towards the periphery. The total number of them is up to 6, but the last rings are very faint (figure 2*a*). Along the ring surfaces the water is sinking and it is slowly ascending in between them, visualized by permanganate particles. This ring pattern after a time τ_{v} was transformed into a vortical structure (figure 2*d*) with a descent along the vortices. The transition between the two states can be seen in figure 2(*b*, *c*). It starts with small wavy perturbations on the rings, on the central one first, which grow and roll-up into vortices as for the Kelvin–Helmholtz shear instability. Evidently, it is this mechanism that causes the vortex formation (Dovzhenko, Novikov & Oboukhov 1979; Chernous'ko 1980; Boubnov 1984). Along the rings the fluid is descending and between them it is ascending, near the surface the fluid moves towards the rings, the convergence lines. Due to the Coriolis force the fluid at different sides of the lines is deflected in opposite directions causing a shear which instability generates the vortices. But this is not the only mechanism of the vortex formation; e.g. inside the central ring vortices may form almost immediately as in a non-rotating fluid.

We shall now consider some quantitative characteristics of convective rings.

(i) The time for formation of the first ring τ_{r} does not depend on the rotation rate Ω, but is determined by the layer depth h and the heat flux f. The timescale in a viscous fluid is h^2/ν. Figure 3 presents the dependence of τ_{r} on this scale divided by the cubic root of the Grasshof flux number:

$$Gr_f = \frac{\alpha g f h^4}{\rho c_p \nu^3} = Ra_f Pr^{-2}. \tag{3.1}$$

The power exponent here, as well as everywhere below, was determined by using logarithmic coordinates for $\tau_{\mathrm{r}} \nu h^{-2}$ and Gr_f. The 87 measured times τ_{r} presented in figure 3 gave the linear regression in seconds as

$$\tau_{\mathrm{r}} = 2.06\, h^2 \nu^{-1} Gr_f^{-\frac{1}{3}} + 20.3 \tag{3.2}$$

with the determination coefficient $r^2 = 0.87$ and correlation coefficient $r = 0.93$. The statistically rather well determined relationship (3.2) can be explained as follows. Inspection of (3.1) and (3.2) shows that τ_{r} should not depend on the viscosity. Remember also that for the convection the vertical velocity

$$w(z) = a(\epsilon z)^{\frac{1}{3}}, \tag{3.3}$$

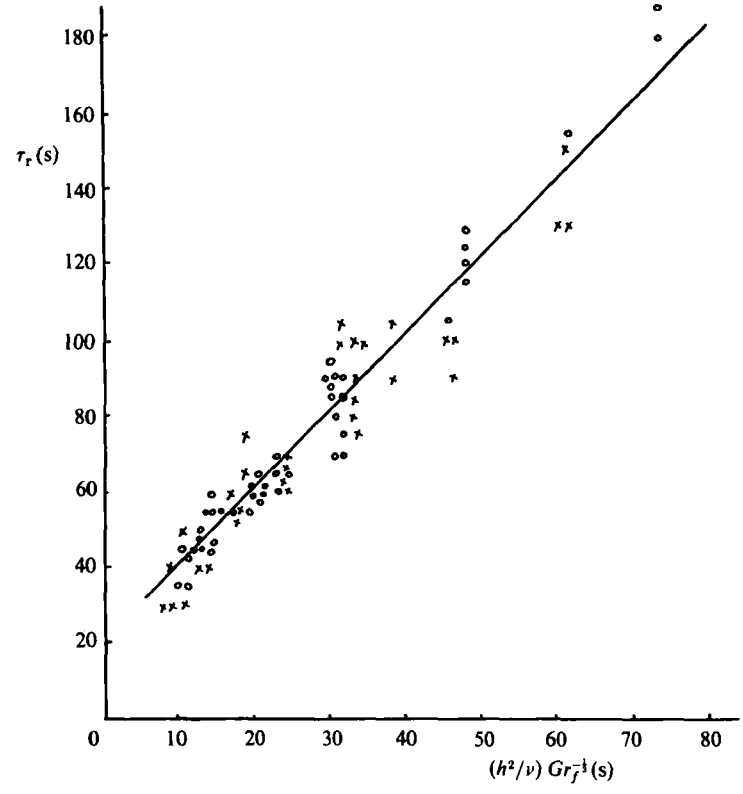

FIGURE 3. Time of formation of the first central ring τ_r, in s, versus the viscous timescale h^2/ν times the inverse cubic root of the Grasshof number: ○, round vessel; ×, square vessel.

where $a \approx 0.4$ for $\Omega = 0$, and the rate of kinetic-energy dissipation is (at $Nu \gg 1$ and also for $\Omega \neq 0$, see Golitsyn 1979):

$$\epsilon = \frac{\alpha g f}{\rho c_p}. \tag{3.4}$$

Define, averaged with height, velocity

$$\bar{w} = \frac{1}{h}\int_0^h w(z)\,\mathrm{d}z = \frac{3a}{4}(\epsilon h)^{\frac{1}{3}}. \tag{3.5}$$

Using (3.4) we may rewrite the Rayleigh flux number as†

$$Ra_f = \frac{\epsilon h^4}{k^2 \nu} = Gr_f Pr^2. \tag{3.6}$$

The first term on the right of (3.2) may now be written as

$$\tau_r = 2.06\left(\frac{h}{\bar{w}}\right)\left(\frac{4}{3a}\right) = \frac{c_1 h}{\bar{w}}, \quad c_1 = 6,87. \tag{3.7}$$

† Equation (3.6) suggests a number of interpretations of the Rayleigh flux number. For example, neglecting the multiplyer Pr^2 it is the non-dimensional rate of the kinetic-energy generation (dissipation) for convection, if the velocity scale is chosen, as is usual, as k/h. The Grasshof number Gr_f is the fourth power of the ratio of the depth h to the Kolmogorov microscale $l_K = \nu^{\frac{3}{4}}\epsilon^{-\frac{1}{4}}$.

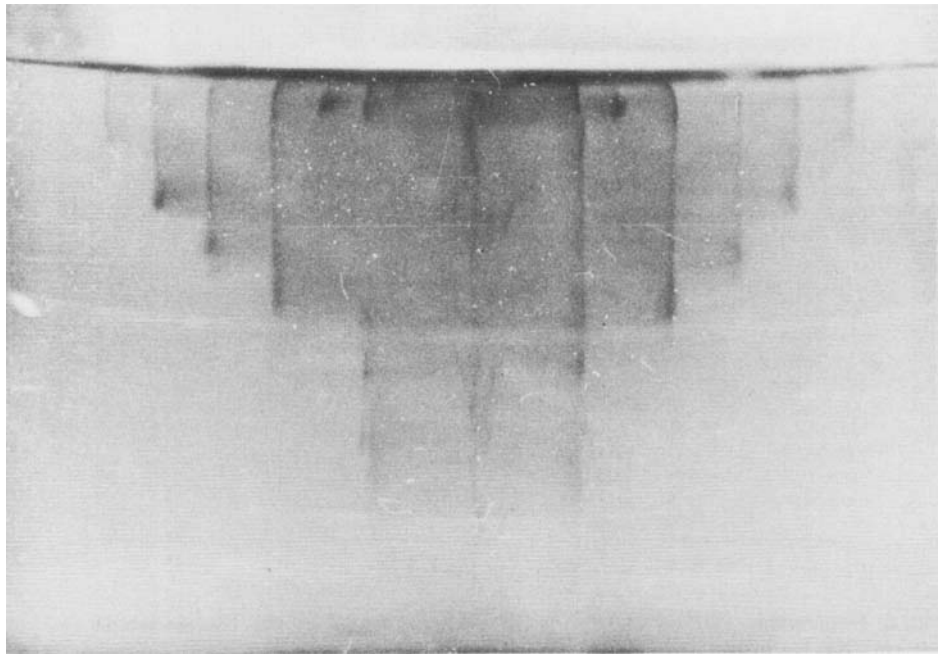

FIGURE 4. Side view of the ring convective pattern: the depth of the rings decreases outwards from the centre.

Therefore the time of the first ring formation τ_r is found to be of the order of the convective time scale $h/\bar{w}$. This fact together with the absence of rings at smaller Ω shows that the process of (the first) ring formation is a result of complicated interplay between spin-up of water and convection. The spin-up time is

$$\tau_{su} = h(\nu\Omega)^{-\frac{1}{2}} = \frac{\Omega^{-1} Ta^{\frac{1}{4}}}{\sqrt{2}}. \tag{3.8}$$

It varied in our experiments from about 10 s to several minutes. The fact that we did not observe rings at smaller Ω, when vortices start to form everywhere, suggests that if the spin-up time (3.8) is large compared with some convective scale t_c of order $h/\bar{w}$ the rings may not form. When we have vortices but no rings, they are chaotic in space and time, and the regime will be called irregular (or turbulent) vortex grid (see §§4 and 5 below). Rings usually evolve into a regular grid.

(ii) Figure 4 presents a side view of the rings at one stage of their evolution. The depth of descent of the fluid in the rings at each moment $\tau_r < t < \tau_v$ is approximately inversely proportional to the rings' distance from the centre. If so, the area of sheets along which the fluid descends is about constant for every sheet. This may reflect the formation times of the sheets.

(iii) There exists a minimum diameter d_m of the central ring which depends on the angular velocity ($d_m \propto \Omega^{-1}$), depth and heat flux. A lengthscale in rotating fluids is the Ekman scale l_E defined by (1.5). We treated the data from 48 measurements presented in figure 5 using

$$d_m = c_2 l_E Ta^{-\frac{1}{4}} Ra_f^{\alpha} = c_2' \left(\frac{l_E^2}{h}\right) Ra_f^{\alpha}, \quad c_2' = \frac{c_2}{\sqrt{2}}. \tag{3.9}$$

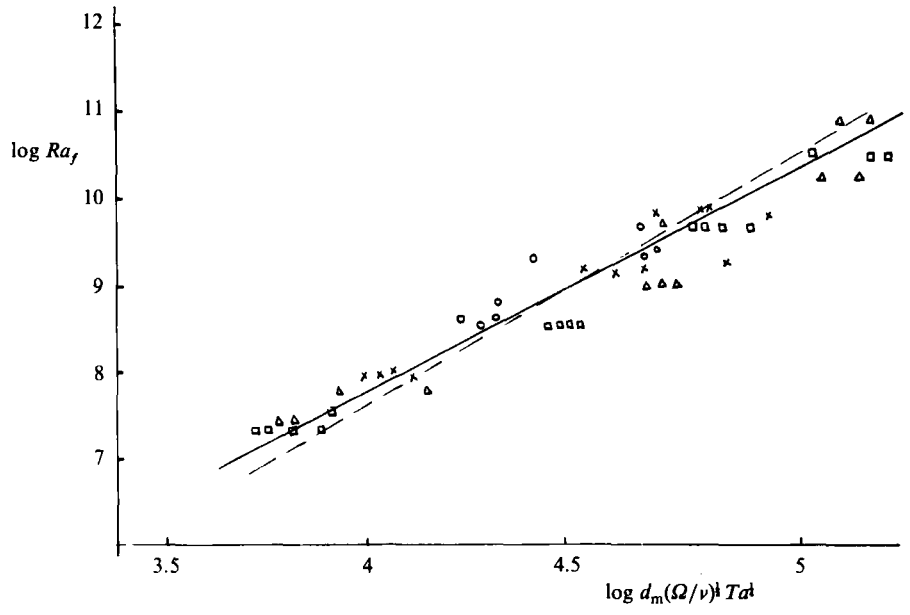

FIGURE 5. Dependence of the central ring diameter d_m scaled by the Ekman length (1.5) on the Taylor and Rayleigh flux numbers: ——, the regression (3.9); – – – –, (3.10); □, $f = 85$ W m^{-2}; ○, 180 W m^{-2}; ×, 500 W m^{-2}; △, 1000 W m^{-2}.

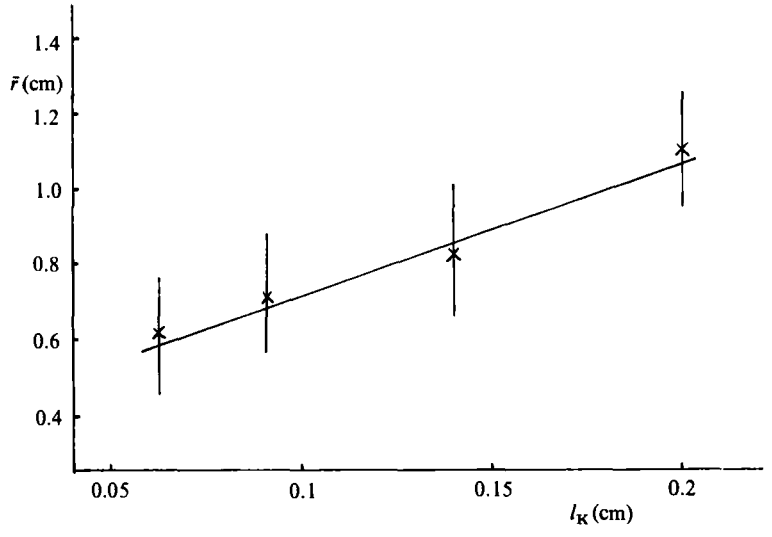

FIGURE 6. Dependence of the mean distance between the rings on the Kolmogorof microscale l_K; each point is an average of about twenty individual measurements, bars indicate r.m.s. deviations.

The linear regression gives $c_2 = 6.2$, $\alpha = 0.4$ with $r^2 = 0.87$. We cannot comment on this dependence except to note that the dependence of d_m on molecular parameters is rather weak: $d_m \propto \nu(k^2\nu)^{-\frac{2}{5}} = Pr^{\frac{3}{5}} k^{-\frac{1}{5}}$. A simpler, but not very easily understood interpretation would arise if $\alpha = \frac{1}{3}$. Then with $d_m \propto \Omega^{-1}$ we would have, taking into account (3.4)–(3.6),

$$d_m \propto (\epsilon h)^{\frac{1}{3}} \Omega^{-1} Pr^{\frac{2}{3}}, \tag{3.10}$$

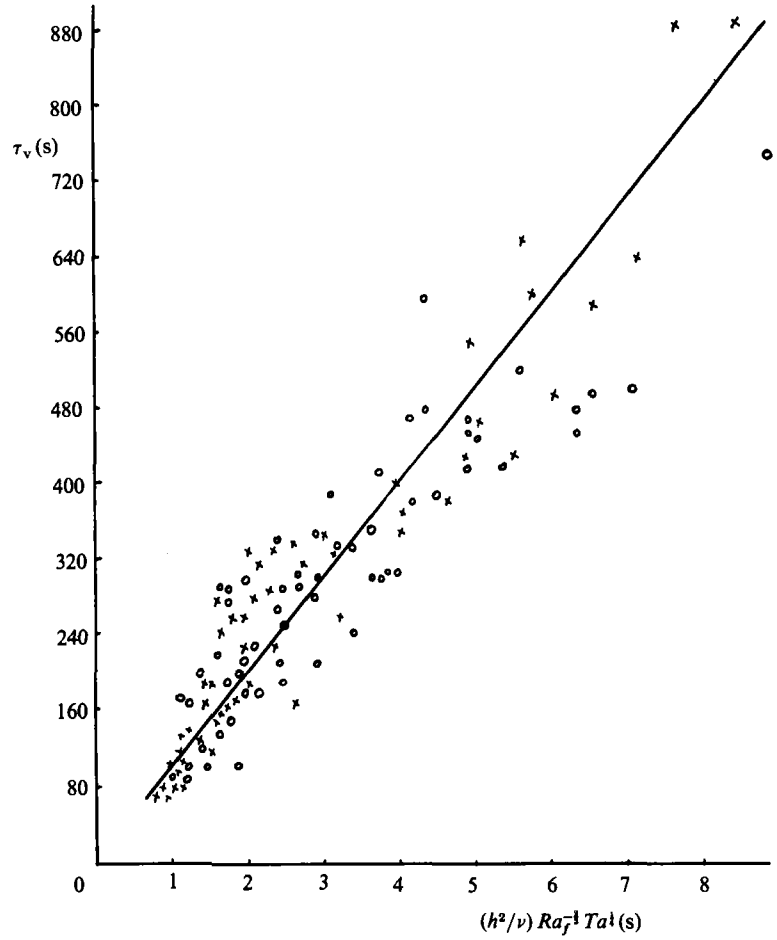

FIGURE 7. Dependence of the time of formation of the convective vortex pattern τ_v on the determining parameters: ○, round vessel; ×, square vessel.

which would show an interplay between convection and rotation. The dashed line in figure 5 shows the dependence $d_m \propto Ra_f^{\frac{1}{3}}$ which may also fit our data. We did not expect before treating this data as in (i), that the viscosity dependence would be weak or might be absent altogether.

(iv) The distance between the rings r varied in our experiments from 0.4 to 1.3 cm. In every case one may see a tendency for r to decrease with an increase in the radius of the rings. We checked in particular whether there is any function for r like the distance between the roots of $J_0(r)$, the zero-order Bessel function (the principal eigenmode for cylindrical geometry), but it was not clear that this was the case. Moreover, in experiments repeated with exactly the same external parameters the value of r may vary by 50%. Therefore we averaged all the distances and used $\bar{r}$ determined for identical sets of external conditions. There was a clear dependence on the heat flux, but no dependence on the depth h and angular velocity Ω. In these circumstances the only lengthscale is the Kolmogorov microscale $l_K = \nu^{\frac{3}{4}}\epsilon^{\frac{1}{4}}$ and we may look for a relationship of the type

$$\bar{r} = c_3 l_K + c_4, \tag{3.11}$$

where $c_3 = 3.3$, $c_4 = 0.39$ cm and $l_K = h\,Ra_f^{-\frac{1}{4}}\,Pr^{\frac{1}{2}}$, see (3.6). The relation leading to (3.10) is presented in figure 6, where every point with error bars (r.m.s. deviations) corresponds to about twenty individual measurements. It is worth emphasizing that both the minimum ring diameter and their mean spacing are not governed by the Ekman scale (1.5) according to our results.

(v) Having existed for some time up to 15 min the rings rolled-up into vortices, see figure 2(*a–d*). The time of the vortex formation, taken from switching-on the turntable up to the disappearance of the last ring, depends on the heat flux, depth and angular velocity. All these dependences can be described by, see figure 7,

$$\tau_v = c_5\,h^2\nu^{-1}\,Ra_f^{-\frac{2}{3}}\,Ta^{\frac{1}{4}}, \tag{3.12}$$

where $c_5 = 101$ and the determination coefficient $r^2 = 0.84$ ($r = 0.92$) for 116 points. In this treatment we also included results obtained when vortices were formed without the ring stage. We cannot present any simple interpretation for this dependence. Clearly viscosity, convection and rotation all play a part here.

4. Vortical convection

4.1. *Types of vortex convective grids*

Three types of vortex patterns are possible depending mainly on the values of the similarity criteria. In this subsection we discuss them only in qualitative terms and a quantitative analysis will be given in §§4.2 and 5.

4.1.1. *Regular convective vortex grid*

Centres of vortices are in the vertices of equilateral triangles, see figure 8, though one may observe some 'dislocations' there. All the vortices are cyclonic, as was previously observed and explained by Nakagawa & Frenzen (1955), because water in them sinks and the convergence intensifies the angular momentum there. The positions of vortices are similar to theoretical predictions (Chandrasekhar 1953, 1961), but there is an important difference in the flow organization compared with the Chandrasekhar case of two both free-stress boundaries, the only case for which he describes the flow field. In the latter case the fluid sinks in the centre of a hexagon and ascends in its vertices. We observed the ascend along some cylindrical or conical surfaces in the centres of which there is an intense vortex with a strong vertical descent motion. Such a structure of vortices is clearly seen by Nakagawa & Frenzen (1955) in their figure 1 for a slightly irregular vortex grid viewed from above, where central dots, intense vortices, are seen inside fainter circles. Traces of such a structure may be also seen around some vortices in figure 8(*a*) (plane view) and (*b*) (inclined view).

Such a picture can be stationary for a long time (e.g. a working day), if the boundary conditions are kept stationary. However, at higher Rayleigh numbers there may be an interaction between a pair of adjacent vortices without appreciable influence on the positions in the grid of other neighbouring ones.

4.1.2. *Convective vortex grid with strong interactions*

After the formation of the convective grid the interactions at even higher Rayleigh numbers may be not only between occasional pairs of vortices, but also between more distant vortices. As a result, strong vortices are formed or strong mixing occurs destructing the grid in certain areas of the vessel. After some time the grid or a strong vortex may form anew in the area of mixing and the interactions start again.

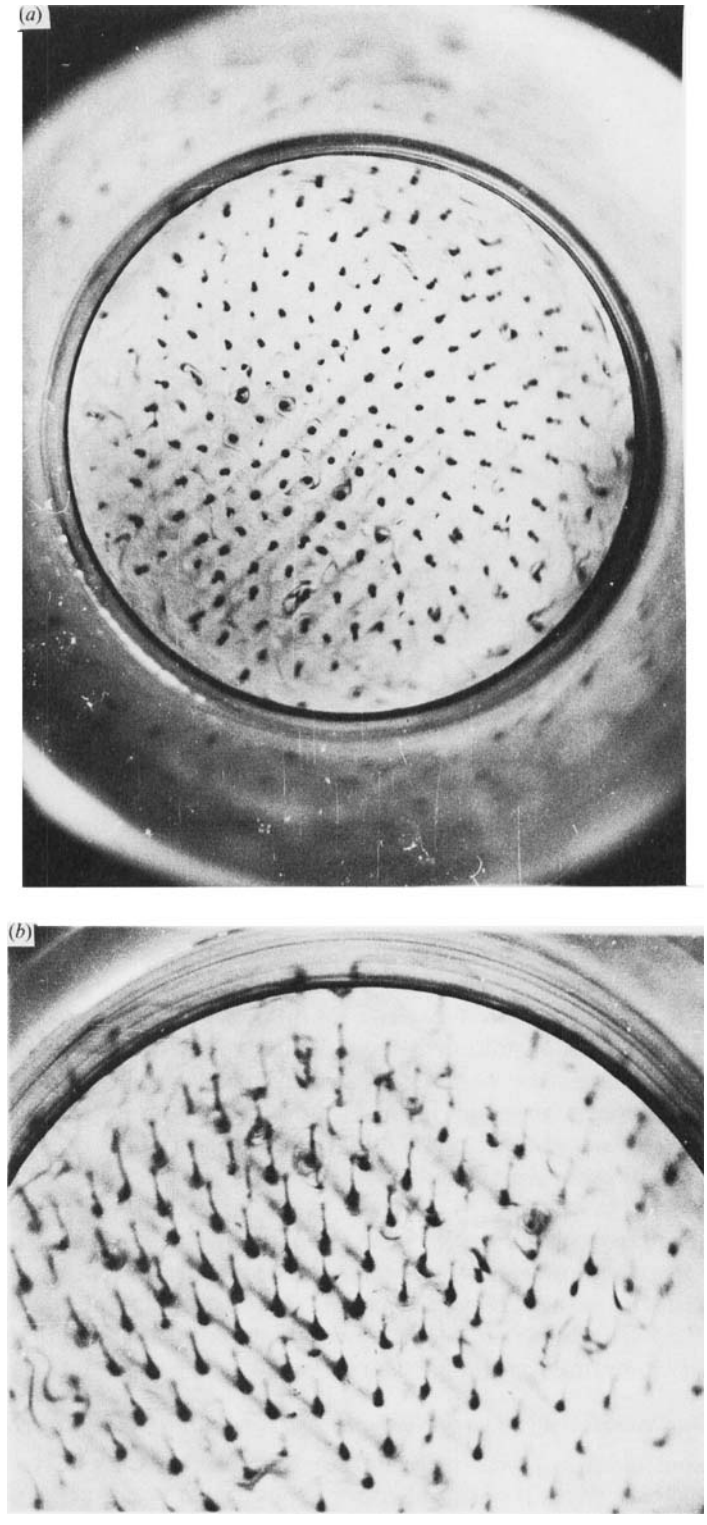

FIGURE 8. Convective vortex grid: (*a*) plane view, (*b*) inclined view; $Ra_f = 7.1 \times 10^7$, $Ta = 5.9 \times 10^8$.

FIGURE 9. An example of an irregular convective vortex pattern; $Ra_f = 2.0 \times 10^8$, $Ta = 7.1 \times 10^7$.

We shall describe the interactions of vortices in some detail in §6. We note that all of the more or less regular grids were formed from the rings reported in §3.

4.1.3. *Irregular vortex pattern*

At even higher Rayleigh numbers or smaller Taylor numbers (for quantitative details see §4.2) an irregular vortex pattern is formed as a result of the decay of the semi-regular vortex grid, which may exist for only a short time. An irregular pattern may form without a semi-regular grid stage similar to the one described under §4.1.2. When there are no rings, the vortices formed in about a minute (see lower left part of figure 7) are always irregular in space and move along more or less random trajectories. Irregular vortices are much less intense than in the vortex grid, they are less concentrated in space and descent velocities are markedly slower. Their mutual interaction is much weaker.

An example of irregular vortex convection is presented in figure 9, where the visualization uses aluminium powder (to emphasize contrasts a black disk was placed on the bottom of the vessel). Regimes similar in appearance but with fewer vortices were described by Hopfinger *et al.* (1982) when they studied the influence of rotation on mechanically generated turbulence (see also §5).

4.2. *Transition from regular vortex grids to irregular convection*

As we have mentioned in §1 the criterion for the onset of convective motion in the rotating fluid layer (1.6*b*) or its equivalent for the two rigid boundaries (Chandrasekhar 1961) was first checked experimentally by Nakagawa & Frenzen (1955). Though their individual points scatter considerably, a dependence of the (1.6*b*) type was well

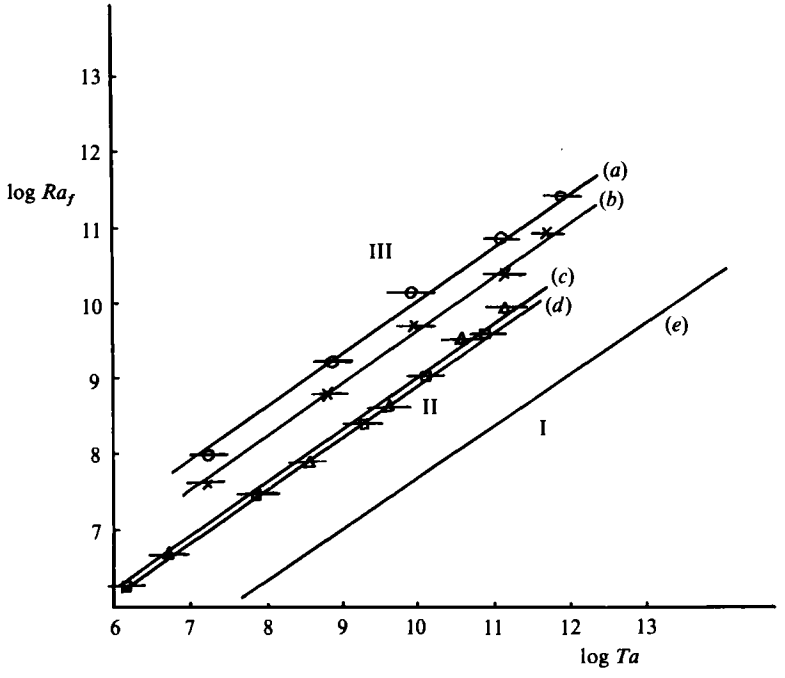

FIGURE 10. Transition from the regular convective vortex grid to an irregular one for different values of the heat flux: (*a*) $f = 1960$ W m^{-2}; (*b*) 690 W m^{-2}; (*c*) 140 W m^{-2}; (*d*) 85 W m^{-2}; (*e*) the neutral stability curve (1.6*b*); transition at every point was achieved by decreasing Ω. The right end of a line near each point corresponds to a regular grid, the left end to an irregular one; I refers to the fluid in rigid rotation, II to the regular grid, III the irregular regime.

confirmed for $10^5 < Ra < 10^8$ and $10^6 < Ta < 2 \times 10^{10}$. However, Rossby (1969) observed for $Ta > 10^6$ and also for two rigid boundaries, using different techniques to determine Ra_{cr}, an increasing deviation from a (1.6*b*)-type dependence. His results are better described as $Ra_{cr} \propto Ta^n$ with $n = 0.57$ (determined by us from his figure 11) instead of $\frac{2}{3}$. The causes for that are still not clear. We shall present supportive evidence for the linear theory in the appropriate region of Ra_f and Ta in §5, where we consider the vortex spatial density or their spacing.

The overall picture is the following: if we, for a sufficiently large Taylor number Ta = const., increase the Rayleigh flux number by increasing the heat flux f, then after a state of no motion – the rigid rotation, region I in figure 10 – we obtain a new stationary state – the vortex convective grid (the ring structure is a transient phenomenon) situated at region II in figure 10. Further increase of f causes the appearance of irregular vortex patterns, region III, which may be also called turbulent vortex convection. The transition from the regular grid to the irregular one on the parameter plane (Ra_f, Ta) is rather gradual, determining a whole transitional region (of a strip-like shape), which is described in §4.1.2. The transition from I to III can also be performed at Ra_f = const. by decreasing the Taylor number Ta thereby easing the rotational constraint. We found that this was best done by keeping the water temperature T_w constant and decreasing the rotation rate. Ra_f and Ta are varied by changing the fluid depth but keeping the water temperature constant for each series of measurements.

The results of determining transitions between states II and III are presented in

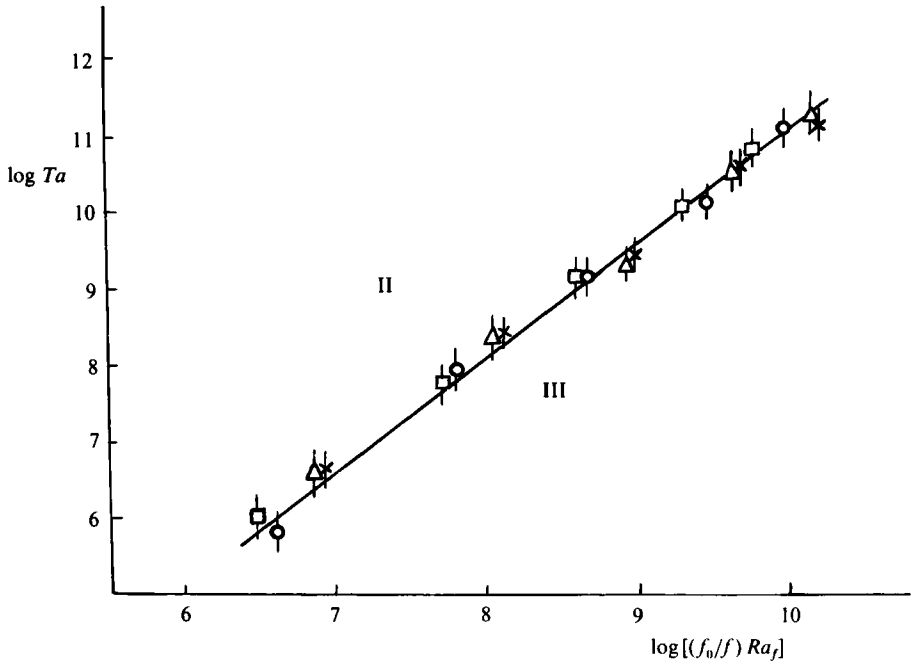

FIGURE 11. The same as in figure 10, but the coordinate $\log Ra_f$ is replaced by $\log[(f_0/f)\,Ra_f]$ where $f_0 = f_3 = 140$ W m^{-2}.

figure 10. The ends of lines correspond to a particular regime: at the left end the regime is fully irregular and at the right completely regular. It was a surprise that for each value of the heat flux f a different curve was obtained: (a, b, c, d) but for every curve

$$Ra_{f2i} = c_i\, Ta^{\frac{2}{3}}, \tag{4.1}$$

as for the stability curve (1.6b) dividing regions I and II. The larger the heat flux the higher is a particular transitional line Ra_{f2i} ($i = 1, 2, 3, 4$) as a function of Ta. Clearly an additional non-dimensional parameter depending on f must enter, and the only possibility is the Nusselt number, $Nu \propto f$, and defined by (1.4). Unfortunately we cannot determine it directly from our measurements because we do not know the temperatures at the water-layer boundaries. Using the definition (1.3) we may rewrite (4.1) as

$$Ra_2\, Nu_i = c_i\, Ta^{\frac{2}{3}}. \tag{4.2}$$

Because the index i refers to the particular heat flux f_i, we omit it from the ordinary Rayleigh number (2 refers to the transition from state II to state III: from regular to irregular convection). At this point we may recall again the work by Rossby (1969). His figure 11, mentioned at the beginning of this subsection, also presents the results of measurements of the Nusselt number as isolines in (Ra, Ta) coordinates for water and his figure 13 for mercury. Both of his figures show that for $Ta > 10^7$ and for $Nu \lesssim 10$ in water, and for $Nu \lesssim 3$ in mercury, these isolines are proportional to $Ta^{\frac{2}{3}}$. He presents results only for $Ta < 10^8$ in the first case and for $Ta < 10^9$ in the second case, but the patterns in both pictures strongly suggest that for higher Ta isolines for larger values of Nu tend also to be proportional $Ta^{\frac{2}{3}}$. So we may assume that in (4.2) not only f_i but also Nu_i is constant.

To check these possibilities we plotted $(f_0/f_i)\,Ra_{f2i}$ as a function of the Taylor number, where $f_0 = f_3 = 140$ W m^{-2}. The results are presented in figure 11. The fact

that all four experimental curves coalesce into a single one shows that in (4.1), or (4.2), coefficients c_i are indeed proportional to f_i, or Nu_i with the same proportionality coefficient. This shows that the transition from a regular to an irregular regime is governed more naturally by the ordinary Rayleigh number Ra, rather than by the flux number Ra_f.

The straight line in figure 11 corresponds to

$$\frac{f_0}{f_i} Ra_{f2i} = c_6 Ta^{\frac{2}{3}}, \tag{4.3}$$

where $c_6 = 464 \pm 113$, if we consider the ends of segments in figure 11. Clearly the value of c_6 depends on the choice of f_0. By multiplying both sides of (4.3) by $h/\rho c_p k \Delta T$ we may rewrite it, accounting for (1.4), as

$$\frac{Ra_{f2i}}{Nu_i} = \frac{c_6}{Nu_0} Ta^{\frac{2}{3}} \tag{4.4}$$

or, using (1.3), as

$$Ra_2 = \frac{c_6}{Nu_0} Ta^{\frac{2}{3}} = c_6' Ta^{\frac{2}{3}} \tag{4.5}$$

where Nu_0 is an unknown constant and $c_6' < 464 \pm 113$, because $Nu > 1$ for the transition under study.

We can try to reduce the estimate of the value of c_6'. The lowest heat flux that we achieved at which the transition from II to III was still observed was $f_4 = 85$ W m^{-2}. This reduces the upper estimate of c_6' to 282 ± 69. If we could know the value of Nu_0 for this flux and/or performed successful measurements at even smaller values, we could further reduce the value of c_6'.

We may compare (4.5) with (1.6*b*) and obtain

$$Ra_2 = c_6'' Ra_{\mathrm{cr}}, \tag{4.6}$$

where the multiplyer $c_6'' < (282 \pm 69)/8.7 = 33 \pm 8$. We see that if the usual Rayleigh number is some 30 times (or perhaps less) greater than the first critical Rayleigh number (having in mind the difference in boundary conditions – see end of §1), then the convection is irregular.

There is another interesting interpretation of the same transition processes which can be obtained from relationship (4.3), i.e.

$$\Omega_{\mathrm{p}} = \frac{2\Omega}{h} = \left(\frac{\alpha g f_0 \nu^{\frac{1}{3}}}{c_6 \rho c_p k^2} \right)^{\frac{3}{4}} = c_7(T_{\mathrm{w}}), \tag{4.7a}$$

where the value of c_7 is a function of the temperature only because the molecular constants depend on T_{w}. On the left of (4.7) we have the density of the total potential vorticity. If $\Omega_{\mathrm{p}} > c_7$ the vortex grid is stable; if the inequality is reversed the grid is unstable (because of the gradual nature of the transition we should allow for a range of values of c_7 to make a definite statement). Equation (4.7*a*) illustrates again the role of rotation in flow stabilization, but for the transition between regular and irregular regimes. To our knowledge such a view of stability problems in rotating flows employing the potential vorticity has not received much attention.

We may non-dimensionalize (4.7*a*) by introducing formally $\epsilon_0 = \alpha g f_0 / c_6 \rho c_p$ where $f_0/c_6 = 140$ W m^{-2}/464 $= 0.3$ W m^{-2}. Then we form the Kolmogorov scales of length, $l_{\mathrm{K}} = \nu^{\frac{3}{4}} \epsilon_0^{-\frac{1}{4}}$ and time $\tau_{\mathrm{K}} = (\nu/\epsilon_0)^{\frac{1}{2}}$ to obtain

$$\Omega_{\mathrm{p}}' = \frac{2\Omega \tau_{\mathrm{K}} l_{\mathrm{K}}}{h} = Pr^{\frac{3}{4}}, \tag{4.7b}$$

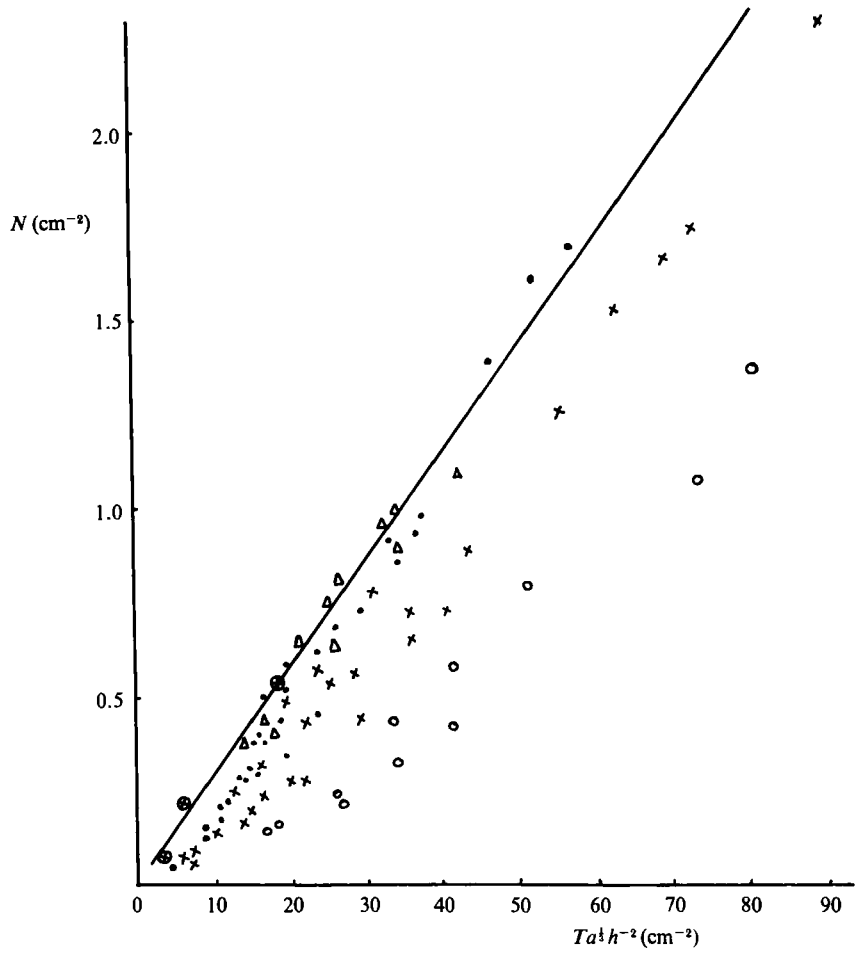

FIGURE 12. Dependence of the vortex number density N on $Ta^{\frac{1}{2}}h^{-2}$; ——, equation (1.10): $N = 0.28\,Ta^{\frac{1}{2}}h^{-2}$ from the linear theory; ⊗, points by Nakagawa & Frenzen (1955); △, $f = 85$ W m^{-2}; ·, 140 W m^{-2}; ×, 690 W m^{-2}; ○, 1960 W m^{-2}.

and if $\Omega'_p > Pr^{\frac{3}{2}}$, we have a stable vortex grid, and the converse. One should not ascribe any physical meaning to the value of ϵ_0, or f_0/c_6: it is only a convenient dimensional quantity to simplify (4.7*b*).

5. Structure of convective vortex patterns

The main geometrical parameter of the convective vortex grid, regular or irregular, is the distance between the centres of adjacent vortices d. Non-dimensionalized by the layer depth h it is

$$\frac{d}{h} = 3^{\frac{1}{4}}(2N)^{-\frac{1}{2}}h^{-1}, \tag{5.1}$$

where N is the vortex number density per unit area in an equilateral triangle grid. According to (1.10) $N = 0.028\,Ta^{\frac{1}{3}}h^{-2}$. The value of N was determined by counting vortices on the photographs of the vessel surface and dividing their total number by

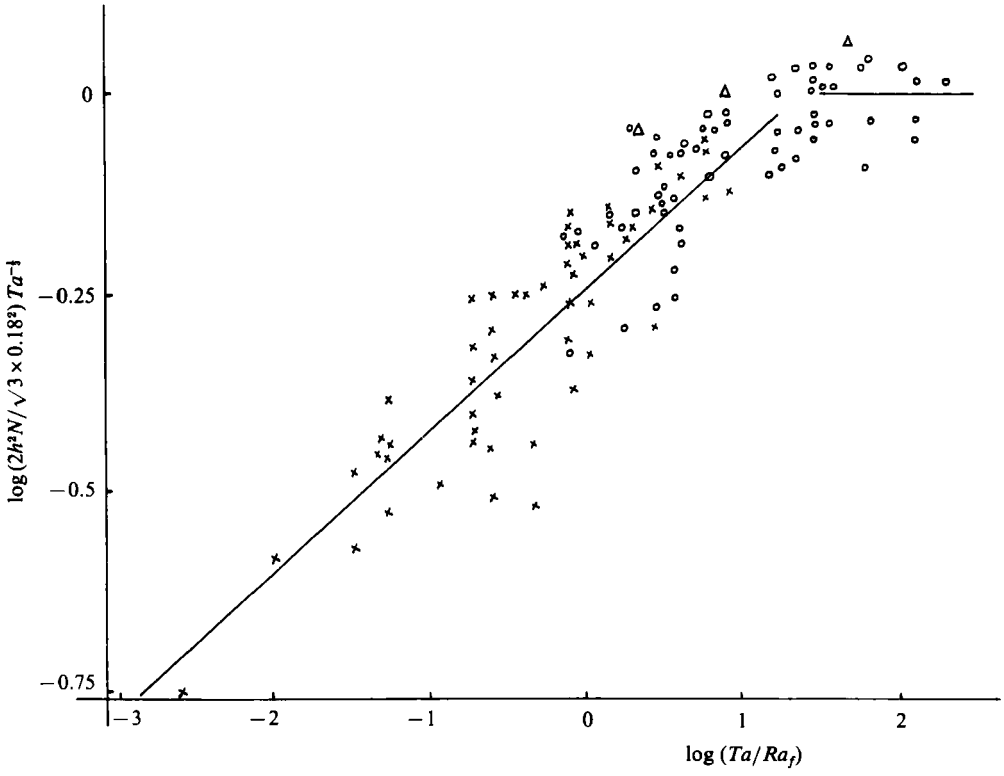

FIGURE 13. Classification of linear and nonlinear convective vortex grids by the dependence of the vortex number density on the external parameters using a special coordinate system, where the straight line parallel to the abscissa corresponds to the linear theory (1.10) and the sloping line to equation (5.2) or the nonlinear regime; △, points from Nakagawa & Frenzen (1955); ○, regular grid; ×, irregular grid.

the surface area. These determinations include some errors, especially for irregular structures or in the presence of vortical interactions. Figures 12–14 present the results of these measurements, first in dimensional form (figure 12), then in a special non-dimensional form (figure 13), and finally in the parameter space (Ra_f, Ta), where figure 14 shows all the flow regimes studied here.

Figure 12 presents results in coordinates (N, $Ta^{\frac{1}{3}}h^{-2}$). The solid line corresponds to the linear-theory (1.10). The three crossed circles are points from Nakagawa & Frenzen (1955). Our points are classified by the value of the heat flux f, because its change in our experiments takes a longer time than changes in h or Ω. The important result from this figure is that most points are well below the theoretical line, though some points, especially at smaller heat fluxes (in fact, smaller Ra_f) agree rather well with the theory when $N \propto \Omega^{\frac{2}{3}}h^{-\frac{2}{3}}$. In the course of intermediate analysis (not presented here) we found that most points agree very well with the relation $N \propto \Omega h^{-\frac{2}{3}}$, where the proportionality coefficient does depend on the value of the heat flux.

Therefore, having in mind these two dependences we plot in figure 13 all our points in the special non-dimensional coordinates, where the ordinate is $y = \lg(2h^2 N Ta^{-\frac{1}{3}} \times 3^{-\frac{1}{2}} \times 0.18^{-2})$ and the abscissa is $x = \lg(Ta/Ra_f)$. In these coordinates if the linear theory holds we have a horizontal line $y = 0$. To fulfill $N \propto \Omega h^{-\frac{2}{3}}$ one should have $y \propto x^{\frac{1}{3}}$. Both asymptotes are shown in figure 13 by segments of straight lines. The circles correspond to regular regimes, crosses to

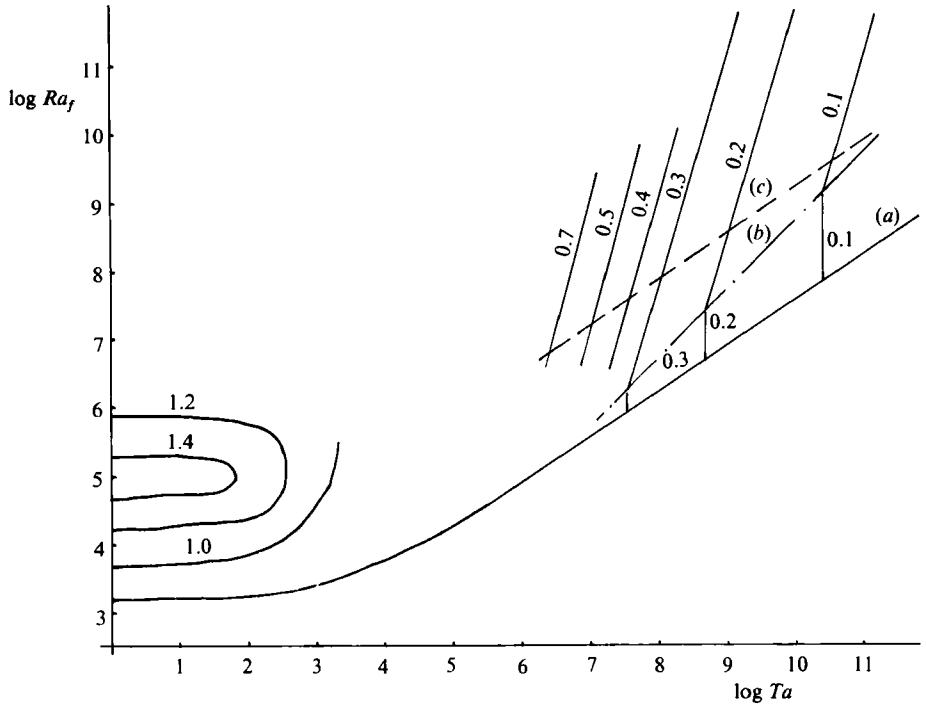

FIGURE 14. Region of the similarity criteria where the experiments were performed. The numbers on the graphs are $a = d/h$ – the non-dimensional distance between the vortices in our experiments ($a \leqslant 0.75$) and between the rolls in Rossby's (1969) experiment (lower part of the figure). (*a*) the stability curve (1.6); (*b*) the separation line between linear (below) and nonlinear regimes; (*c*) one of the curves (4.1) for $f = 140$ W m^{-2} dividing regular and irregular regimes of convection.

irregular ones, triangles are three points by Nakagawa & Frenzen (1955). We can formally determine from the crossing of the two asymptotes that for $Ta/Ra_f > 24.5$ we have the linear regime and for $Ta/Ra_f < 24.5$ a regime which we call nonlinear. There $N \propto \Omega$, the Rayleigh flux numbers are far from their critical stability values and, presumably, the nonlinear effects are important.

The nonlinear regime may be regular or irregular depending on the fulfilment of conditions (4.3) or (4.7), but the whole lower left part of figure 13 corresponds to irregular regimes (crosses), where the influence of rotation is small. The mixing of regular and irregular regimes (circles and crosses) in the central part of figure 13 evidently shows, as found in §4.2, that the value of Ra_f does not conveniently describe these two kinds of regimes. Note that the ratio Ta/Ra_f can be interpreted as $(l_K/l_E)^4$, the fourth power of the ratio of the Kolmogorov microscale to the Ekman scale (see (1.5), (3.6) and the footnote to the latter). The smaller l_K and larger l_E, the larger is the role of convection and the smaller the role of rotation.

In the nonlinear regime the number density of vortices per unit area can be approximated as

$$N = c_8 \Omega \nu^{-1} Ra_f^{-\frac{1}{6}} = c_8 l_E^{-2} Ra_f^{-\frac{1}{6}}, \tag{5.2}$$

where $c_8 = 0.033$, as determined from the linear regression between 104 pairs of N and $\Omega\nu^{-1} Ra_f^{-\frac{1}{6}}$ with the determination coefficient $r^2 = 0.94$ (the correlation $r = 0.97$).

The mean distance between the centres of adjacent vortices is then, from (5.2) and (5.1),

$$d = c_9 l_E Ra_f^{\frac{1}{12}}, \quad c_9 = \left(\frac{\sqrt{3}}{2c_8}\right)^{\frac{1}{2}} = 5.1. \tag{5.3}$$

The linear dependence of the number of vortices on the rotation rate Ω was also noted by Hopfinger *et al.* (1982), who generated turbulence mechanically by oscillating grid in a rotating tank filled with water. It seems that the proportionality $N \propto \Omega$ is a general property of strongly forced flows in rotating fluids. We also obtained a similar relation for the two rigid boundaries of the layer, when the lower boundary was at higher temperature than the upper one with visualization by aluminium powder. Though in this case we could not fully verify the relationship (5.2), by keeping the temperatures of our two thermostats constant and varying Ω however we observed that N was proportional to Ω with a good precision.

Figure 14 summarizes and classifies the results of all our experiments on the plane of the similarity criteria the Rayleigh flux number Ra_f and the Taylor number Ta. The lower curve is the stability curve $Ra_{fcr} = Ra_{cr}$ as a function of Ta according to (1.6) with provision for its dependence on the precise nature of the boundary conditions as discussed at the end of §1. We plotted the isolines of values of the non-dimensional distance between the vortices $a = d/h$ for our experiments (upper right part) and for the experiments by Rossby (1969). For his case a is actually the non-dimensional size of the rolls taken from his figure 7, and the Rayleigh flux number was estimated using his figure 11. In his experiments $a \gtrsim 1$ and in ours $a \leqslant 0.75$. For smaller values of Ta the structure of convection is close to that in a fluid at rest ($\Omega = 0$), which is witnessed by Rossby's experiments and by numerical computations by Sommerville (1971). The line $Ta = 24.5 Ra_f$ marks where the transition to the nonlinear regime (5.2) takes place. It shows that more room appears for the linear regime with the increase of the Taylor number when rotation suppresses nonlinearity.

6. Vortex structure and vortical interactions

In stable regular grids vortices always reach the bottom. With variation in Ra_f and Ta they reach the bottom as practically straight threads or, at some depth, the vortices start rolling out as spirals which reach the bottom. Occasionally we observed perturbations on vortices similar to those reported by Hopfinger *et al.* (1982) in cases of semi-regular grids. In irregular or semi-regular regimes a vortex may not reach the bottom and vortices are seen in a layer with a depth l which is usually the case for larger heat fluxes or larger Ra_f. We determine l as the maximum length of the observed vortices for given values of the external similarity criteria Ra_f and Ta. In our vessel with transparent walls at $f > 600$ W m^{-2} the results of measurements can be described by the relation (see figure 15)

$$\frac{l}{h} = c_{10} Ta^{\frac{1}{8}} Ra_f^{-\frac{1}{4}},$$

where according to the linear regression $c_{10} = 0.39$, $r^2 = 0.88$ for 48 points. This dependence is fulfilled for $4 \times 10^9 < Ra_f < 2 \times 10^{11}$ and $10^6 < Ta < 10^8$. At smaller Ra_f the dependence on it is much less appreciable.

When we move into the region of irregularity, we first observe separate local violations of the symmetry; however in general vortices are immovable. With further

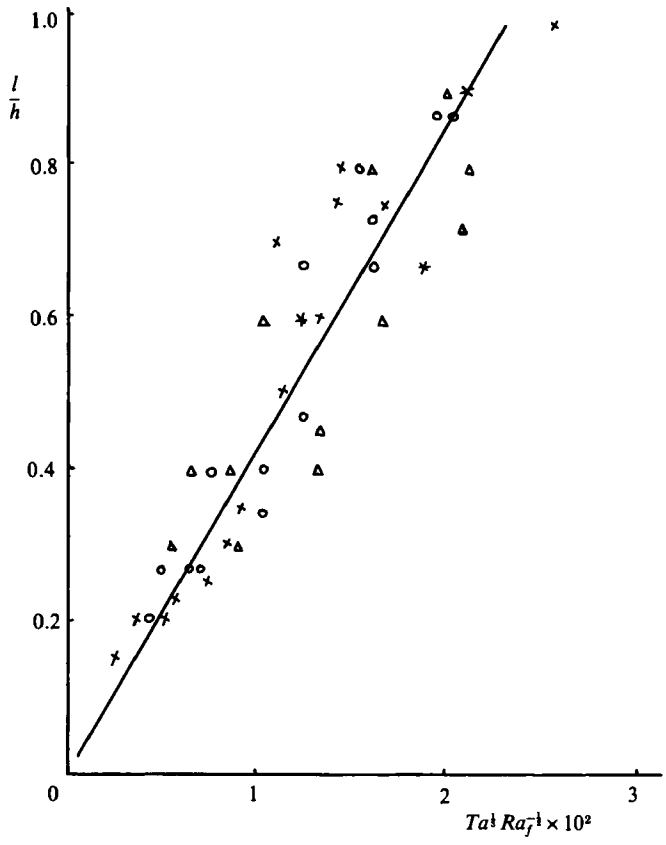

FIGURE 15. Dependence of non-dimensional length of vortices on external parameters; ×, $h = 20$ cm; ○, 15 cm; △, 10 cm; *, 6 cm.

increase of the Rayleigh flux number, or decrease of the Taylor number pair interactions of some adjacent vortices appear: first a vortex pair starts to rotate around a common axis as in the classical theory of two-dimensional vortices, then the vortices begin to interlace, particularly their upper parts, forming a double helix, and finally they coalesce into one vortex of greater intensity. These three stages are marked 1, 2 and 3 in figure 16. The process of collapse of the double helix also starts from its upper part. After the collapse the vortex formed weakens and occupies the place in the grid of one of the two original vortices, and at the vacant place a new vortex starts to grow. After a time, similar interactions can be observed in another place, sometimes one may see several such interactions in various places simultaneously. This picture relates to stable vortex grids. If the grid is eventually unstable, as described in §4.1, it is the vortical interactions which lead to a decay of the regular structure soon after its formation.

We tried to determine the dependence of the time of the vortex interactions τ_{vi} on the external parameters. We define the beginning of the time interval as the moment when the vortex pair is seen to start its rotation, and the end of it as the moment when the upper parts of the two vortices have coalesced. The values of τ_{vi} measured by a stop-watch are found to be independent, on average, of the general rotation rate Ω, but do depend on the heat flux and layer depth. We did not succeed

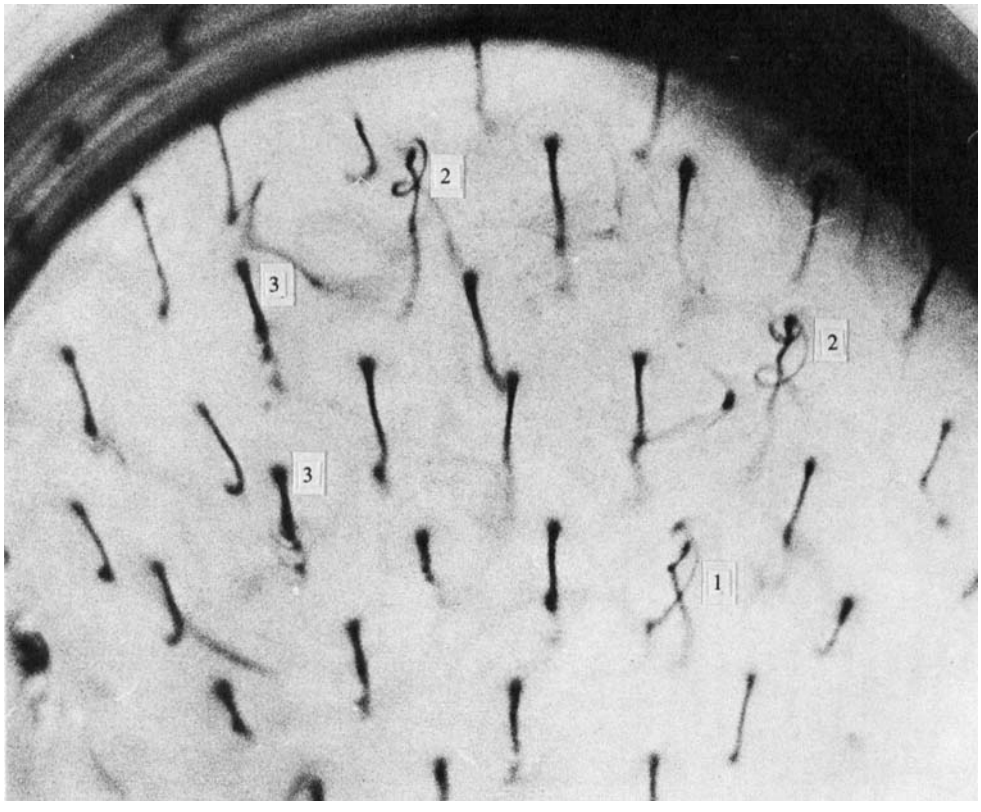

FIGURE 16. Vortex interactions in the convective grid: 1, interlacing of two vortices; 2, formation of a double helix; 3, coalescence of the vortices; $Ra_f = 1.05 \times 10^8$, $Ta = 5.9 \times 10^8$.

f (100 W m^{-2})	2				5				10.8		
h (cm)	3	6	10	20	3	6	10	15	3	6	10
τ_{vi} (s)	26	41	63	140	16	20	26	42	11	13	18
$Ra_f 10^{-6}$	6.6	105	810	13000	24	380	2940	14800	71.6	1140	8800

TABLE 1. Time of the vortex interactions τ_{vi} for three values of the heat flux f, and various layer depths h, averaged over the angular velocity Ω (several values for each case)

in finding any single dependence on the Rayleigh flux number, therefore we present results of our determinations of the time τ_{vi} in table 1.

We see from table 1 that the time τ_{vi} increases with the depth, but decreases with the heat flux.

7. Some qualitative experiments

We shall describe two sets of qualitative experiments that reveal the features of convection in rotating fluids.

We carried out several experiments with the turntable placed on an inclined plane

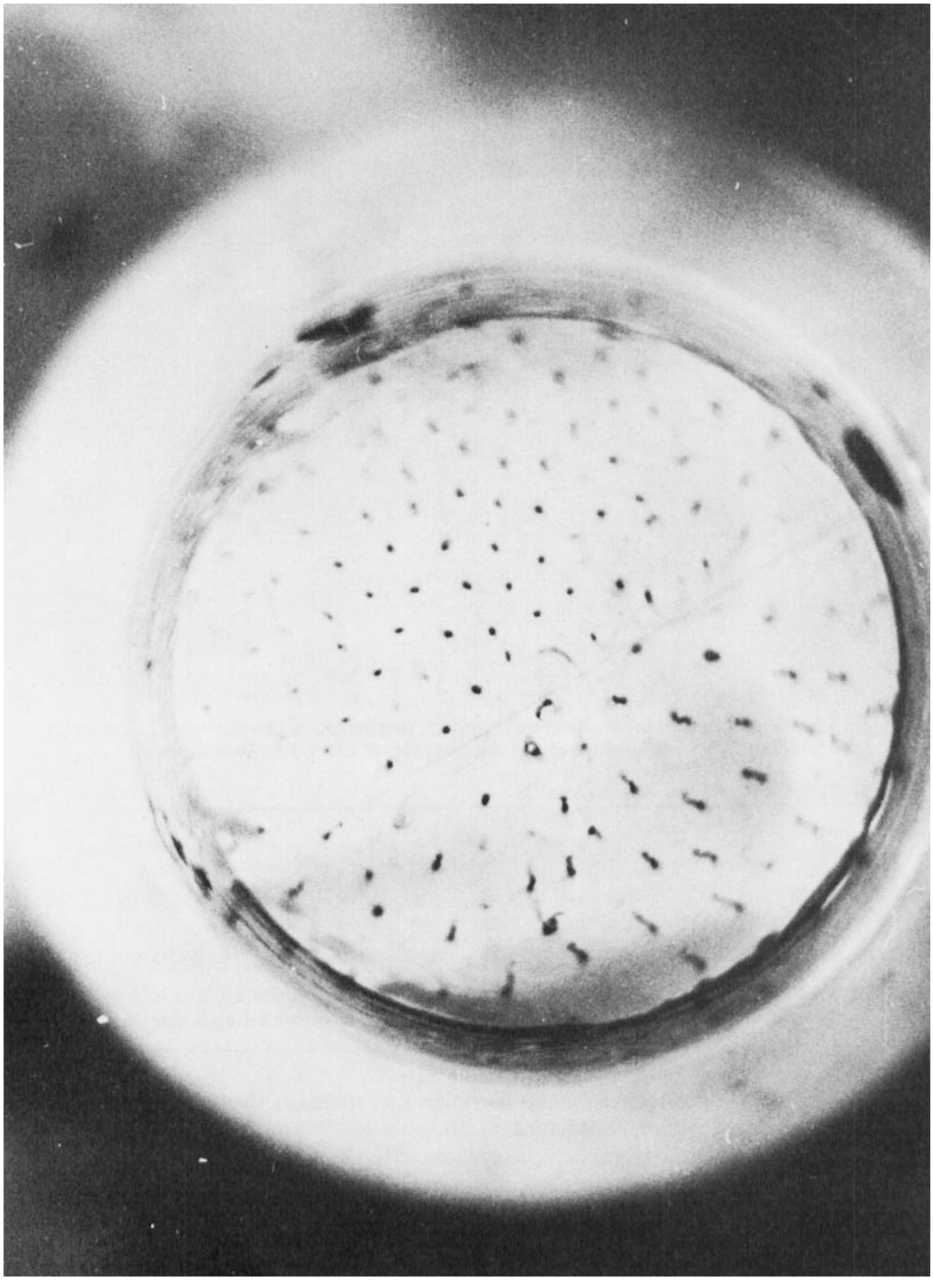

FIGURE 17. The vortex convective patterns for the vessel with a stepped bottom: one half $h = 2$ cm, the other half $h = 10$ cm.

with the inclination angle up to 30°. The vessel, which was filled with water, had a rigid cooled upper lid and a heated bottom. The convective grid was formed with the vortex axes along the direction of the angular velocity in full accord with the Proudman–Taylor theorem. The results of Busse & Carrigan (1974) described in §1 are relevant here because they present the limiting case when the volume force was perpendicular to the rotation axis, with the flow patterns still aligned along Ω.

Some experiments were performed in a vessel with a stepped bottom. According to (1.10) and the results in §5 the spacings of the grid must be different in parts of different depth. The case presented in figure 17 shows the convection in the vessel, one half of which has $h = 2$ cm, and the other half $h = 10$ cm. The difference in distance between the vortices is clearly seen. At the interface one can see the vortex interactions caused by the difference in the structures, which cause grid destruction at certain places and formation of some more intensive vortices. But away from the boundary both grids are very regular. This implies a strong stability of convective grids and that vortical interactions are short range, because defects of the grids are clear only near the interface (especially, in the more dense 2 cm deep grid, for which the Rayleigh flux number is $(10/2)^4$, 625 times less than for the other grid).

8. Conclusions

We have performed experiments on convection in rotating water with a free surface and analysed the results for a wide range of the similarity criteria Rayleigh flux number and Taylor number. But the range is far to low for any direct geophysical applications. The experiments have revealed a rich picture of flow patterns and regimes, but many aspects and details of the picture have remained virtually untouched or understudied. For instance, the structure of vortices and cells, briefly mentioned in §4.1, seems to be very intriguing. The extension of measurements to higher values of Ra_f and Ta is obviously necessary, e.g. in the light of potential contradictions hinted by the results presented in figures 10 and 13 and more clearly seen in figure 14; for example, the line $24.5\,Ra_f = Ta$ found to divide linear and nonlinear, but still regular, regimes is about to intersect the lines (4.1), $Ra_{fzi} = C_i Ta^{\frac{2}{3}}$ separating regular and irregular regimes. Clearly, measurements of temperature and direct determinations of the ordinary Rayleigh number and Nusselt number are required to settle directly the problem of transition to irregular regimes. To fulfil this programme one needs a larger tank and turntable and a much more sophisticated measurement technique. This work appears to be only the very beginning of systematic studies in the subject.

Nevertheless, our experiments show the following characteristic features of convection in rotating fluids:

(i) formation of various convective vortex patterns, regular or irregular;

(ii) formation of regular patterns in a layer cooled from the free surface is preceeded by an intermediate stage, the ring structure in a symmetrical geometry, which is formed apparently from interaction of the non-uniform velocity field in the fluid spin-up with the convection caused by cooling from the free surface;

(iii) the characteristic spacing of the vortex grid depends on the regime, linear or nonlinear, determined by the ratio of the Taylor and Rayleigh heat flux numbers: if $Ta/Ra_f \gtrsim 25$, we have the linear regime with spacing d determined by the linear theory of convective instability in rotating fluids of Chandrasekhar (1953, 1961) and by Nakagawa & Frenzen (1955), when $d \propto \Omega^{-\frac{1}{3}}$; in the nonlinear regime when $Ta/Ra_f < 25$ we find $d \propto \Omega^{-\frac{1}{2}} \propto l_E$, the Ekman length, as in the case of mechanically

generated turbulence in a rotating tank (Hopfinger *et al.* 1982). However, the flow structure of our observed vortex patterns is different, even in the linear regime, from that theoretically predicted for both boundaries stress-free: all our vortices in a triangular grid are of the same cyclonic sign, in which fluid sinks and ascends along some cylindrical surfaces surrounding the vortices, while in the theory the vortices in the centres of hexagonal cells are cyclonic and anticyclonic at their vertices, where the fluid ascends;

(iv) the transition from a regular vortex grid to an irregular one is through the vortex interaction and is rather gradual in the parameter space; it appears to be governed by a value of the ordinary Rayleigh number (better, a range of the Rayleigh numbers at a given Taylor number), which is found to be proportional to $Ta^{\frac{2}{3}}$, as is the first transition Rayleigh number from the state of rest (rigid rotation); the ratio of the two transitional numbers is in the range 25–40;

(v) the vortex interactions, the basic mechanism transforming the regular convective grids into irregular ones, have three stages: rotation of a vortex pair around a common axis, interlacing of the vortices forming a double-helix structure and collapse of the structure into one more-intense vortex.

We wish to express our sincere gratitude to Academician A. M. Oboukhov for support of this work and several useful discussions, and also to two referees, whose comments and questions required clarification of many points, which considerably improved the presentation of the material.

REFERENCES

Boubnov, B. M. 1984 Laboratory model of convection in a rotating annulus in conditions of horizontally and vertically inhomogeneous heating. *Izv. Atmos. Oceanic Phys.* **20**, 767–770.

Busse, F. N. & Carrigan, C. R. 1974 Convection induced by centrifugal buoyancy. *J. Fluid Mech.* **62**, 579–592.

Chandrasekhar, S. 1953 The instability of a layer of fluid heated below and subject to Coriolis forces. *Proc. R. Soc. Lond.* A **217**, 306–327.

Chandrasekhar, S. 1961 *Hydrodynamic and Hydromagnetic Stability*. Clarendon.

Chernous'ko, Yu. L. 1971 Experimental studies of microconvection in laboratory conditions. *Izv. Atmos. Oceanic Phys.* **7**, 724–727.

Chernous'ko, Yu. L. 1980 Experimental studies of two-dimensional flows with horizontal shear in a rotating system. *Izv. Atmos. Oceanic Phys.* **16**, 285–289.

Dikarev, S. N. 1983 On the influence of rotation on the convection structure in a deep homogeneous fluid. *Dokl. Akad. Nauk SSSR* **273**, 718–720 (in Russian).

Dovzhenko, V. A., Novikov, Yu. V. & Oboukhov, A. M. 1979 Modelling the process of vortex generation in axially-symmetric azimuthal field by MHD-method. *Izv. Atmos. Oceanic Phys.* **15**, 1199–1202.

Ginsburg, A. I., Dikarev, S. N., Zatsepin, A. G. & Fedorov, K. N. 1981 Phenomenological features of convection in fluids with a free surface. *Izv. Atmos. Oceanic Phys.* **17**, 289–295.

Ginsburg, A. I. & Fedorov, K. N. 1978 Cooling of water at free and forced convection. *Izv. Atmos. Oceanic Phys.* **14**, 79–87.

Golitsyn, G. S. 1979 Simple theoretical and experimental study of convection with some geophysical applications and analogies. *J. Fluid Mech.* **95**, 567–608.

Golitsyn, G. S. 1981 Structure of convection at fast rotation. *Dokl. Akad. Nauk SSSR* **261**, 317–320 (in Russian).

Golitsyn, G. S. & Grachev, A. A. 1980 Velocities and heat and mass transfer at convection in two-component medium. *Dokl. Akad. Nauk SSSR* **255**, 548–552 (in Russian).

GOLITSYN, G. S. & GRACHEV, A. A. 1986 Free convection of multi-component media and parameterization of air–sea interaction at light winds. *Ocean–Atmos. Interaction* **1**, No. 1 (to appear).

GOLITSYN, G. S., GRACHEV, A. A. & LAPSHIN, A. I. 1984 Heat and mass transfer at free convection in a multi-component gas medium. *Dokl. Akad. Nauk SSSR* **277**, 858–862 (in Russian).

GRACHEV, A. A. 1983 Convective cooling of fluids from the free surface. *Izv. Atmos. Oceanic Phys.* **19**, 513–523.

HOPFINGER, E. J., BROWAND, F. K. & GAGNE, Y. 1982 Turbulence and waves in a rotating tank. *J. Fluid Mech.* **125**, 505–534.

JEFFREYS, H. 1928 Some cases of instability in fluid motion. *Proc. R. Soc. Lond.* A **118**, 195–208.

KOSCHMIEDER, E. L. 1967 On convection under an air surface. *J. Fluid Mech.* **30**, 9–15.

MARTYNENKO, O. G. & SOKOVISHIN, YU. A. 1982 Free convection heat exchange. *Handbook, Minsk, Nauka i Technika* (in Russian).

NAKAGAWA, Y. & FRENZEN, P. 1955 A theoretical and experimental study of cellular convection in rotating fluids. *Tellus* **7**, 1–21.

ROSSBY, H. T. 1969 A study of Bénard convection with and without rotation. *J. Fluid Mech.* **36**, 309–337.

SOMMERVILLE, R. C. J. 1971 Bénard convection in a rotating fluid. *Geophys. Fluid Dyn.* **2**, 247–262.

VARGAFTIK, N. B. 1972 Handbook on thermophysical properties of gases and liquids. Moscow: Nauka (in Russian).

VERONIS, N. B. 1968 Large-amplitude Bénard convection in a rotating fluid. *J. Fluid Mech.* **31**, 113–139.